Articles

^{15}N Backbone Dynamics of Ferricytochrome b_{562}: Comparison with the Reduced Protein and the R98C Variant†

Michael Assfalg,‡ Lucia Banci,‡ Ivano Bertini,*,‡ Simone Ciofi-Baffoni,‡ and Paul D. Barker§

Magnetic Resonance Center and Department of Chemistry, University of Florence, Sesto Fiorentino, Italy, and Centre for Protein Engineering, MRC Centre, Hills Road, Cambridge CB2 2QH, United Kingdom

Received January 22, 2001; Revised Manuscript Received July 12, 2001

ABSTRACT: The backbone dynamics of ferricytochrome b_{562}, a four-helix bundle protein from *Escherichia coli*, have been studied by NMR spectroscopy. The consequences of the introduction of a *c*-type thioether linkage between the heme and protein and the reduction to the ferrous cytochrome have also been analyzed. ^{15}N relaxation rates R_1 and R_2 and ^{1}H−^{15}N NOEs were measured at proton Larmor frequencies of 500 and 600 MHz for the oxidized and reduced protein as well as for the oxidized R98C variant. In the latter protein, an "artificial" thioether covalent bond has been introduced between the heme group and the protein frame [Arnesano, F., Banci, L., Bertini, I., Ciofi-Baffoni, S., de Lumley Woodyear, T., Johnson, C. M., and Barker, P. D. (2000) *Biochemistry 39*, 1499−1514]. The ^{15}N relaxation data were analyzed with the ModelFree protocol, and the mobility parameters on the picosecond to nanosecond time scale were compared for the three species. The three forms are rather rigid as a whole, with average generalized order parameters values of 0.87 ± 0.08 (oxidized cytochrome b_{562}), 0.84 ± 0.07 (reduced cytochrome b_{562}), and 0.85 ± 0.07 (oxidized R98C cytochrome b_{562}), indicating similar mobility for each system. Lower order parameters (S^2) are found for residues belonging to loops 1 and 2. Higher mobility, as indicated by lower order parameters, is found for heme binding helices α1 and α4 in the R98C variant with respect to the wild-type protein. The analysis requires a relatively long rotational correlation time (τ_m = 9.6 ns) whose value is accounted for on the basis of the anisotropy of the molecular shape and the high phosphate concentration needed to ensure the occurrence of monomer species. A parallel study of motions in the millisecond to microsecond time scale has also been performed on oxidized wild-type and R98C cytochrome b_{562}. In a CPMG experiment, decay rates were analyzed in the presence of spin-echo pulse trains of variable spacing. The dynamic behavior on this time scale is similar to that observed on the sub-nanosecond time scale, showing an increased mobility in the residues connected to the heme ligands in the R98C variant. It appears that the increased protein stability of the variant, established previously, is not correlated with an increase in rigidity.

Protein molecules are not rigid entities but experience a variety of motions over a wide range of time scales and amplitudes. They vary from fast local oscillations about bonds to slower cooperative movement of segments of the overall structure (*1*). Molecular motions can influence the binding of substrate, the catalytic process, and the mode of interaction with other macromolecules. In addition, it is clear that dynamic properties are related to protein stability and folding (*2*). NMR spectroscopy is of particular value for the investigation of molecular motions of proteins in that it provides complete information about the dynamic behavior under physiological conditions (*3*). For X-ray crystallography, at least some fluctuations may be dampened significantly by crystal packing contacts (*4*).

Measurement of ^{15}N relaxation rates has become an important means of studying the backbone dynamics of proteins in solution (*5*−*7*). They can be conveniently analyzed on the millisecond to microsecond and picosecond to nanosecond time scales (*8*−*13*). Relaxation measurements represent a natural continuation of structural studies, providing useful information about the mechanism of the biological function and about protein stability.

Our interest here is focused on cytochrome b_{562} (cyt b_{562}) from *Escherichia coli*, a periplasmic, 12 kDa protein containing a single *b*-type heme moiety. The iron is essentially low-spin, six-coordinate, with methionine and

† This work was supported by the European Community (TMR-LSF Contract HPRI-CT-1999-00009 and TMR Contract FMRX-CT98-0230) and by Italian CNR (Progetto Finalizzato Biotecnologie 97.04327.CT14).

* To whom correspondence should be addressed: Magnetic Resonance Center and Department of Chemistry, University of Florence, Via Luigi Sacconi, 6, 50019 Sesto Fiorentino, Italy. Phone: +39-055-4574272. Fax: +39-055-4574271. E-mail: bertini@cerm.unifi.it.

‡ University of Florence.

§ MRC Centre.

10.1021/bi0101300 CCC: $20.00
Published on Web 10/06/2001

histidine providing the axial ligands. It cycles between Fe(II) and Fe(III) oxidation states. The heme, which is not bound covalently to the protein matrix, is present in two orientations, the A (major) and B (minor) forms. They differ by a 180° rotation around the $\alpha-\gamma$ meso direction. The structure of the oxidized holoprotein has been determined by X-ray crystallography to a resolution of 1.4 Å (*14*) and by NMR spectroscopy (*15*), revealing a four-helix bundle fold. To continue the characterization of this protein, the dynamic properties of form A have been analyzed over a time range of different time scales.

Recently, the structure of the R98C variant cytochrome b_{562} (R98C cyt b_{562}) has also been determined by NMR spectroscopy (*16*). In the A orientation, the heme is attached covalently through its 2-vinyl group to the thiol sulfur of a specifically introduced cysteine. This variant is particularly interesting since cyt b_{562} is the only four-helix bundle cytochrome which does not have a covalently linked heme. The other members of this structurally homologous family, cytochrome c' and c_{556} from photosynthetic bacteria, all have the heme attached to the CXXCH motif in the C-terminal helix (*17*). To determine the effect on the protein dynamics of cross-linking the protein to the heme, a comparison of the mobility data for the wild-type and R98C cyt b_{562} proteins has been made.

In addition, the dynamic properties have been analyzed for form A of reduced cyt b_{562}. Local mobility has often been proposed to be important in controlling the electron transfer process (*18*−*23*). It is suggested to influence both the molecular recognition process and the reorganization energy λ, both features being necessary to achieve electron transfer in biological systems. Therefore, a comparison of the mobility of the protein in two different oxidation states is particularly useful.

Differences in generalized order parameters obtained from ^{15}N relaxation analyses were used to estimate an upper limit of the contribution of backbone dynamics to the entropy changes occurring upon reduction or chemical modification (*24*, *25*).

In the present case, the data indicate that both the reduced cytochrome and its oxidized R98C variant are stabilized significantly with respect to unfolding, relative to the oxidized wild-type (WT) protein [$\Delta\Delta G_{D-N}^{H_2O} = 25$ and 5.6 kJ/mol, respectively (*16*, *26*)]. We have investigated whether the origins of these differences in stability can be related to differences in dynamic behavior.

MATERIALS AND METHODS

Sample Preparation. ^{15}N-labeled *E. coli* cyt b_{562} was prepared as described previously (*15*, *27*). Expression and purification of the Arg98Cys variant of cyt b_{562} were performed as described previously (*27*) with the modifications introduced by Arnesano et al. (*16*). The samples used for NMR spectroscopy contain 1.8 mM protein and 500 mM phosphate buffer at pH 4.8 in 90% H_2O and 10% D_2O. The low protein concentration and the high ionic strength are such that aggregation or dimerization of the protein is avoided (*28*). Confirmative measurements were also performed on samples at lower concentrations. The reduced form of cyt b_{562} was obtained by adding sodium dithionite and a catalytic amount of a hydrogen-saturated solution of *Desulfovibrio vulgaris* iron hydrogenase to the deoxygenated solution of cyt b_{562}, which was then saturated with hydrogen. This method allows the sample to be kept reduced for a longer period of time than with only the addition of sodium dithionite in an argon atmosphere. Furthermore, when partial reoxidation was observed, hydrogen bubbling restored the completely reduced sample. To check the invariance of the sample during each experiment, the volumes of the peaks in HSQC spectra collected at the beginning and at the end of each set of experiments were compared.

NMR Spectroscopy. NMR experiments were carried out at 298 K, on both a Bruker Avance 500 and a Bruker Avance 600 NMR spectrometer operating at proton Larmor frequencies of 500.13 and 600.13 MHz, respectively.

The pulse sequences used to measure ^{15}N longitudinal and transverse relaxation rates, R_1 and R_2, were those previously described (*5*, *29*), appropriately modified to eliminate cross correlation between dipolar and chemical-shift anisotropy (CSA) relaxation mechanisms (*30*−*32*) and with pulsed field gradients to suppress the water signal. Longitudinal and transverse relaxation rates were obtained using delays in the pulse sequence (T) of 10, 70, 150, 250, 380, 540, 740, 1000, 1350, 2000, and 3000 ms and 7.6, 15.2, 30.4, 60.8, 76, 106.4, 136.8, 167.2, 182.4, 212.8, and 258.4 ms, respectively. A refocusing delay of 450 μs was used in the transverse relaxation measurements. For heteronuclear ^{1}H−^{15}N NOE measurements, two-dimensional (2D) spectra were acquired using the water flip-back method to suppress the water resonance (*33*). For the three species, two NOE spectra with ^{1}H saturation and one without saturation were collected. In total, 2048 × 256 data points (2048 × 512 for reduced cyt b_{562}) were collected using 8 (R_1), 16 (R_2), and 64 (NOE) scans for each experiment. The recycle delay was set to 2.5 s for the longitudinal and transverse relaxation measurements and to 3 s in the NOE experiments. ^{1}H saturation was maintained for 2.5 s in the NOE experiments with saturation. The correction of NOE values for incomplete ^{1}H T_1 recovery (*33*) has been calculated, and it turned out to be insignificant (with respect to experimental error) for all the residues that were analyzed.

To monitor slow conformational exchange processes, transverse relaxation rates of backbone ^{15}N nuclei under relatively weak effective fields were measured at 600 or 500 MHz for both oxidized wild type and R98C cyt b_{562} proteins. The experiments were performed as a function of the spin-echo delay in T_2-CPMG experiments using a pulse sequence described in the literature (*31*, *34*) and using the WATERGATE sequence (*35*) for water suppression. Sets of experiments were carried out at six CPMG refocusing delays (τ_{CPMG}) (450, 550, 700, 850, 1000, and 1150 μs), which allow the observation of exchange between conformational substates with average lifetimes ranging from 150 to 400 μs. Relaxation delays varied from 7 to 230 ms, the exact values depending on τ_{CPMG}.

The acquisition time was 120 ms in all experiments. Spectral windows of 34 ppm in the F_1 (^{15}N frequency) dimension and of 14 ppm in the F_2 (^{1}H frequency) dimension were used for oxidized and reduced cyt b_{562}, and windows of 40 (F_1) and 16 ppm (F_2) were used for R98C cyt b_{562}. Data were zero-filled to obtain 2048 × 512 data point matrixes. A commercially available algorithm for linear prediction was used in the indirect dimension to increase

resolution. Quadrature detection in F_1 was achieved by using the TPPI method (*36*).

All NMR data have been processed on a Silicon Graphics workstation using the XWINNMR Bruker Software. Integration of cross-peaks for all spectra was performed by using the standard routine of the XWINNMR program.

Analysis of ^{15}N Relaxation Data. Relaxation rates R_1 and R_2 were determined by fitting the cross-peak intensities (I), measured as a function of the delay (T) within the pulse sequence, to a single-exponential decay by using the Levenburg−Marquardt algorithm (*37*, *38*) according to the following equation:

$$I(T) = A + B\exp(-RT) \tag{1}$$

where A, B, and R are adjustable fitting parameters, using a Monte Carlo approach to estimate the error on the rates (*39*−*41*). For R_2, the phase cycle was chosen so that the magnetization relaxes to zero for long relaxation delays. Thus, in this case, A was set equal to zero in the fitting procedure. Heteronuclear NOE values were calculated as the ratio of peak volumes in spectra recorded with and without ^1H saturation. The heteronuclear NOE values and their errors were estimated by calculating the mean ratio and the standard error from the available data sets.

R_1, R_2, and NOE values for ^{15}N spins are determined by dipolar coupling with the attached proton and, for R_1 and R_2, also by the chemical shift anisotropy of the nitrogen spins. The equations for these rates, in terms of spectral density functions [$J(\omega)$], are reported in the literature (*42*). R_2 can also contain a contribution originating from exchange, R_{ex}.

The experimental longitudinal and transverse relaxation rates and the heteronuclear NOEs have been analyzed with the ModelFree 4.0 program (*43*), within the Lipari−Szabo approach (*9*). This program models the overall rotational diffusion using a diffusion tensor **D**. In the analysis presented here, we have used both isotropic and axially symmetric models to account for the global rotational motion (*44*−*46*). Initial estimates for the overall tumbling correlation time and the local correlation times for the NH vector of each residue were derived from the measured R_2/R_1 ratios. The diffusion tensor of the molecule was initially estimated by fitting the local correlation times for the NH vector of each residue to an input structure with the program *quadric_diffusion*, available from the Web site of A. G. Palmer, III. These parameters were then optimized at the final steps of the relaxation rate fitting (see below). In this analysis, care was taken to remove from the input relaxation data those NHs having an exchange contribution to the R_2 value or exhibiting large-amplitude internal motions on a time scale longer than a few hundred picoseconds, identified from low NOE values, as inclusion of these data would bias the calculated tensor parameters (*5*, *47*). The input structures for *quadric_diffusion* and ModelFree calculations were the energy-minimized average solution structures of oxidized cyt b_{562} and R98C cyt b_{562} (*15*, *16*). The structure of the reduced form of cyt b_{562} is assumed to be similar to that of the oxidized one, for the present purpose.

Within the ModelFree approach, various terms of the spectral density function, $J(\omega)$, can be taken into account with a maximum of three adjustable parameters to reproduce the experimental rates. These are (under the assumption that the tumbling of the molecule in solution is isotropic)

$$J(\omega) = \frac{2}{5}\left[\frac{S^2\tau_m}{1+(\omega\tau_m)^2}\right] \tag{2a}$$

$$J(\omega) = \frac{2}{5}\left[\frac{S^2\tau_m}{1+(\omega\tau_m)^2} + \frac{(1-S^2)\tau'}{1+(\omega\tau')^2}\right] \tag{2b}$$

$$J(\omega) = \frac{2}{5}\left[\frac{S^2\tau_m}{1+(\omega\tau_m)^2} + \frac{(S_f^{\,2}-S^2)\tau'}{1+(\omega\tau')^2}\right] \tag{2c}$$

where $\tau'^{-1} = \tau_m^{-1} + \tau_e^{-1}$, τ_m is the correlation time for molecular reorientation, and τ_e is the correlation time for internal motions, faster than τ_m but slower than 10 ps. The model described by eq 2c, which is the most general, accounts for the presence of two distinct internal motions occurring on two different time scales, both faster than the overall molecular tumbling. S^2 is the square of the generalized order parameter characterizing the amplitude of the internal motions, and S_f^2 is the square of the order parameter for the fast internal motions characterized by correlation times much smaller than τ_e. S^2 is very sensitive to the distance between the nitrogen and hydrogen atoms and to the ^{15}N CSA used in the ModelFree analysis. Indeed, a decrease of −10 ppm to the ^{15}N CSA decreases the order parameter S^2, obtained from a relaxation analysis at 17.6 T, by ∼4%, which is larger than experimental uncertainties (*45*, *48*). Measurements of ^{15}N dipolar couplings and ^{15}N chemical shifts in solids (*49*, *50*), together with a quantum calculation (*51*), show that a consistent set of values is as follows: $r_{NH} = 1.02$ Å and ^{15}N CSA = −172 ppm (*48*, *52*, *53*). This was used to extract S^2. The three adjustable parameters are S^2 (in eqs 2a−c), τ_e (in eqs 2b and 2c), and S_f^2 (in eq 2c). If an axially symmetric model is used to account for molecular rotational diffusion, the spectral density of eq 2c is given by (*32*, *54*, *55*)

$$J(\omega) = \frac{2}{5}\sum_{j=1}^{3} A_j\left[\frac{S^2\tau_j}{1+(\omega\tau_j)^2} + \frac{(S_f^{\,2}-S^2)\tau_j'}{1+(\omega\tau_j')^2}\right] \tag{3}$$

where $\tau_j'^{-1} = \tau_j^{-1} + \tau_e^{-1}$, $\tau_1^{-1} = 6D_\perp$, $\tau_2^{-1} = 5D_\perp + D_{||}$, $\tau_3^{-1} = 2D_\perp + 4D_{||}$, $A_1 = (3\cos^2\theta - 1)^2/4$, $A_2 = 3\sin^2\theta\cos^2\theta$, $A_3 = {}^3/_4\sin^4\theta$, and θ is the angle between the N−H bond vector and the principal axis of the diffusion tensor (*32*, *54*, *55*). All other symbols have the same meaning as above. The expressions for $J(\omega)$ corresponding to eqs 2a and 2b can be derived from eq 3 as described above for the isotropic case.

To take into account the presence of a contribution to the experimental R_2 relaxation rate, arising from conformational exchange processes, an additional adjustable parameter (R_{ex}), which sums up to the value of R_2, calculated taking into account only the dipolar and CSA contributions, may be introduced. As only three experimental values are available, the maximum number of adjustable parameters is three. Thus, R_{ex} can be introduced only in conjunction with models 2a and 2b. The presence of exchange occurring in a suitable range of rates can also be experimentally determined through transverse relaxation rates measuring these rates at different spin-echo pulse trains of variable spacing (see below).

Fittings were performed by introducing upper limits for S^2 (≤ 1), S_f^2 (≤ 1), and τ_e ($< \tau_m$) and a lower limit for R_{ex} (> 0). No other restraints were used. Model selection in the ModelFree calculations was performed according to a procedure, which is based on χ^2 and F statistics (*43*). The uncertainties in the values of the ModelFree parameter were estimated by Monte Carlo simulations (*43*). To obtain distinct independent measurements of relaxation, data were collected at two different external magnetic fields. The fitting procedure within the ModelFree calculations was performed simultaneously on both data sets. The choice of magnetic fields corresponding to proton frequencies of 500 and 600 MHz was dictated by two contrasting limitations: the resolution (extensive overlap is observed at magnetic fields of <500 MHz) and the errors in estimating the relaxation contribution due to the chemical shift anisotropy which become non-negligible at magnetic fields of >600 MHz (*52*). Once the best model for the molecular motions is selected, the overall τ_m, the $D_{||}/D_{\perp}$ ratio, and the internal motional parameters for each spin are optimized by fitting the experimental relaxation parameters R_1, R_2, and NOE to their equations (*42*) [the Powell minimization algorithm (see section 10.5 of ref *38*) has been used].

It has been previously shown that, if the motions of the NH vectors are not correlated with each other, an upper bound to the contribution of the backbone dynamics to the entropy change occurring between two related states can be calculated from the relation (*24*, *56*)

$$\Delta S = k\sum_n \ln\left[\frac{3 - (1 + 8S_{n,2})^{1/2}}{3 - (1 + 8S_{n,1})^{1/2}}\right] \quad (4)$$

where S is the conformational entropy, k is Boltzmann's constant, and S_n is the square root of the order parameter of the nth NH vector. In this specific case, the initial state (state 1) is the oxidized wild-type cyt b_{562} and the final state (state 2) is either the reduced state of cyt b_{562} or R98C cyt b_{562}.

R_2 Measurements in the Presence of a CPMG Spin-Echo Pulse Train. The effects of spin-echo pulses on transverse relaxation rates due to exchange processes depend on the average field strength produced by the CPMG train. The latter is determined by the repetition time (τ_{CPMG}) with which the 360° pulses are applied:

$$\nu_{eff}\,(s^{-1}) = \frac{1}{2(T_\pi + \tau_{CPMG})} \quad (5)$$

where T_π is the duration of a 180° ^{15}N CPMG pulse (76 μs for the experiments carried out at 600 MHz). When the τ_{ex} of the exchange process is longer than the τ_{CPMG} delay between refocusing pulses, no effect on the relaxation rates is observed.

The contribution of the exchange processes (R_{ex}) to the transverse relaxation rate can be expressed in terms of the CPMG ν_{eff} frequency (*57*):

$$R_{ex} = \frac{k_{ex}}{2} - 2\nu_{eff} \sin h^{-1}\left(\frac{k_{ex}}{\xi} \sin h \frac{\xi}{4\nu_{eff}}\right) \quad (6)$$

where $\xi = (k_{ex}^2 - 4p_A p_B \delta\omega^2)^{1/2}$ and $k_{ex} = 1/\tau_{ex}$. p_A and p_B are the populations of sites A and B, respectively, in a two-site exchange process, and $\delta\omega$ is the difference in the Larmor frequencies between the sites. Numerical simulations indicate that this equation is accurate, provided $(p_A p_B)^{1/2}\delta\omega/k_{ex} < 0.2$; i.e., the exchange process is fast with respect to the chemical shift difference (*57*).

Equation 6 can be simplified in the slow pulsing limit. For ν_{eff} values of $< 0.1k_{ex}$, the exchange-mediated relaxation becomes linearly dependent on the pulse rate (*58*):

$$R_{ex} = \left(1 - \frac{4\nu_{eff}}{k_{ex}}\right) p_A p_B \delta\omega^2/k_{ex} \quad (7)$$

When $\nu_{eff} \ll 0.1k_{ex}$, eq 7 further reduces to the expression for the free precession limit:

$$R_{ex} = p_A p_B \delta\omega^2/k_{ex} \quad (8)$$

When the pulse repetition rate is significantly faster than the exchange rate, R_{ex} contributions are completely suppressed. Experimental limits on the spin-echo delay length are determined by the duty cycle of the transmitter for short delays and the evolution of ^{1}H$-^{15}$N coupling during long delays.

NMRD Measurements. The experimental NMRD profiles of bovine serum albumin were acquired with a Koenig-Brown relaxometer. These experiments measure the ^{1}H water longitudinal relaxation rates as a function of magnetic fields. For this instrument, the range of magnetic fields was from 0.01 to 50 MHz of proton Larmor frequency, with an error of ±1%. The experimental rates are the sum of the rate of bulk water and of that of the water molecules interacting with the protein. The latter rates are modulated by a correlation time which corresponds to the overall tumbling of the molecule. Three sets of measurements were taken on a 3 mM protein sample at pH 5 and 298 K with phosphate concentrations of 0, 5, and 500 mM. Data have been fitted with the model free approach, after the bulk water contribution has been subtracted (*59*).

RESULTS

A Comment on the Possible Effects of Unpaired Electrons. The oxidized forms of cyt b_{562} are paramagnetic, and thus, the effect of the low-spin heme Fe(III) on proton relaxation is expected to be non-negligible (*60*−*62*). However, the effect on nitrogen relaxation is dramatically reduced (by a factor of approximately 100) due to the lower gyromagnetic ratio of the ^{15}N with respect to the ^{1}H nucleus (lower by a factor of 10).

From studies on HiPIPs (*63*) and cytochrome b_5 (*64*, *65*), it was shown that the effect can be safely neglected for ^{15}N nuclei which are more than 7 Å from the paramagnetic center. The backbone ^{15}N nuclei which are within 7 Å of the iron ion, as determined from the average energy-minimized solution structure of oxidized cyt b_{562} (*15*), are those of Met 7 (6.1 Å), Glu 8 (6.7 Å), His 102 (6.7 Å), and Arg 98 (6.6 Å). Met 7 has been excluded from the analysis due to its broad signal (see below). For the other residues, we have estimated the dipolar paramagnetic contribution to nuclear dipolar ^{15}N relaxation, through the Solomon equation (*66*), considering an electronic relaxation time τ_s of 7×10^{-12} s [as estimated for low-spin heme Fe(III) (*61*)]. For a distance of 6.6 Å, the dipolar paramagnetic contribution to longitu-

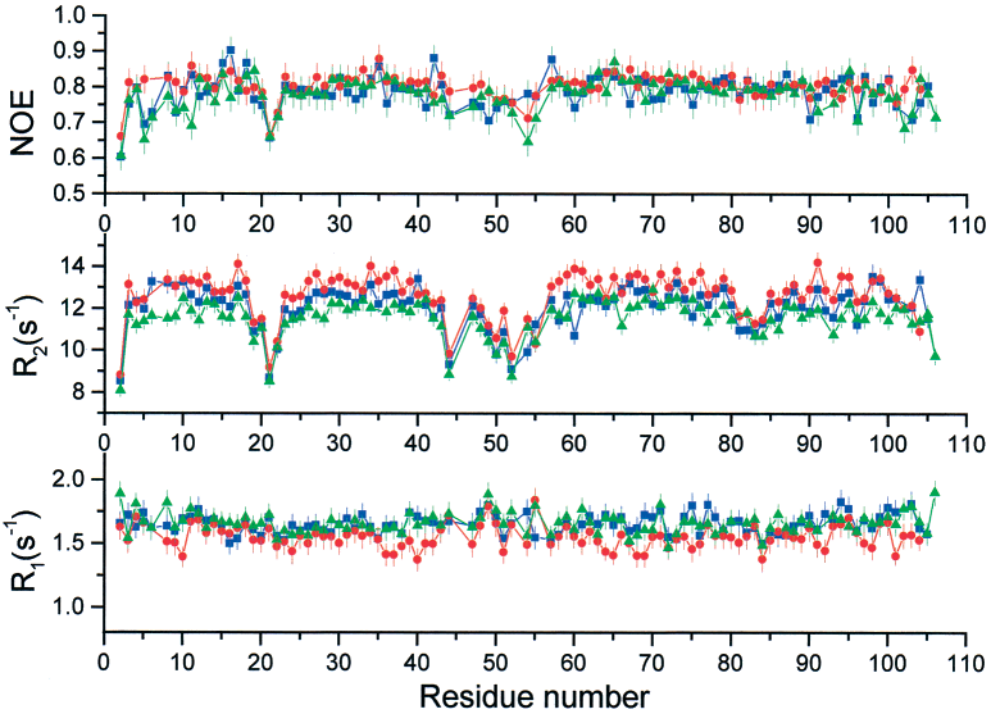

FIGURE 1: Comparison of ^{15}N relaxation parameters vs residue number for oxidized (■), reduced (●), and oxidized R98C (▲) cytochrome b_{562} collected at 500 MHz.

dinal relaxation of the ^{15}N nucleus at 600 MHz was found to be 0.07 s^{-1}, which is very small and within the experimental uncertainty. An analogous conclusion can be made for oxidized R98C cyt b_{562}, based on the fact that the $^{15}N-$iron distances are almost the same as for the wild-type protein.

Relaxation Measurements. Native cytochrome b_{562} is present in two forms (A and B) as a consequence of two different orientations of the heme, one differing from the other by a 180° rotation around the $\alpha-\gamma$ meso direction (*28*). When the signals of the two forms are well separated in the NMR spectra, the mobility data have been collected on the major form A. For the remaining signals, degenerate for the two species, the mobility parameters are the average of those of the two species. However, as degenerate signals in both ^1H and ^{15}N dimensions are indicative of NH moieties with very similar environments, the two forms most likely exhibit similar dynamic behavior. In R98C cyt b_{562}, a single heme orientation is present. However, all preparations we made contain a further species, minor in concentration (intensity ratio of 1:10), which differs in mass by 32 Da (*27*) from the "normal" R98C cyt b_{562} species. Although its origin is still currently unknown, it might originate from oxidation (+2 oxygen atoms) of the Cys residue that forms the thioether bond. The mobility parameters have been collected for the major species with a normal mass.

The experimental R_1, R_2, and $^1H-^{15}N$ NOE values at 500 MHz of the amide ^{15}N nuclei of oxidized and reduced cyt b_{562} and oxidized R98C cyt b_{562} are plotted as a function of the protein sequence in Figure 1. Plots and tables of ^{15}N relaxation data at the two fields are reported in the Supporting Information for the three systems. Average relaxation parameter values at 500 and 600 MHz are reported in Table 1, and they are similar for the three derivatives within error. To ensure that no aggregation is occurring under the experimental conditions described here, relaxation measurements were also performed at 500 MHz on samples of the oxidized wild-type cyt b_{562} at lower protein concentrations (1 and 0.5 mM). Both R_1 and R_2 values are the same, within experimental error, as those measured at a protein concentration of 1.8 mM. For oxidized cyt b_{562}, reliable R_1, R_2, and $^1H-^{15}N$ NOE values have been obtained for 99 residues of the 101 assigned backbone NH resonances. The amide $^1H-^{15}N$ signals of Met 7 and His 102 are too broad to be integrated accurately. The signal of Ala 75 can be integrated only at 600 MHz because sizable overlap is present at lower field strengths. For reduced cyt b_{562}, 98 NH resonances are assigned (unpublished data from this laboratory, same sample conditions as for the oxidized protein); only Asn 6, Tyr 105, and Arg 106 are unassigned in the reduced species. Relaxation rates have been measured for all the assigned residues with the exception of Met 7, whose peak is too broad to be integrated accurately. For oxidized R98C cyt b_{562}, reliable R_1 and R_2 rates for amide ^{15}N and $^1H-^{15}N$ NOE values have been obtained for 98 residues of the 101 assigned backbone NH resonances. The signals of Glu 81 and Glu 92 are overlapped, while the signal of Met 7 is too broad to be integrated accurately.

Table 1: Average R_1 and R_2 Relaxation Rates (s^{-1}) and $^1H-^{15}N$ NOEs for Amide ^{15}N Nuclei Measured at 500 and 600 MHz for Oxidized and Reduced Cyt b_{562} and Oxidized R98C Cyt b_{562}

	oxidized cyt b_{562}	reduced cyt b_{562}	oxidized R98C cyt b_{562}
R_1 (500 MHz)	1.66 ± 0.09	1.54 ± 0.12	1.66 ± 0.08
R_1 (600 MHz)	1.26 ± 0.08	1.18 ± 0.10	1.33 ± 0.08
R_2 (500 MHz)	12.06 ± 1.03	12.62 ± 1.06	11.54 ± 0.89
R_2 (600 MHz)	12.67 ± 1.16	12.72 ± 1.37	12.51 ± 1.17
$^1H-^{15}N$ NOE (500 MHz)	0.78 ± 0.05	0.80 ± 0.03	0.78 ± 0.05
$^1H-^{15}N$ NOE (600 MHz)	0.82 ± 0.04	0.81 ± 0.05	0.84 ± 0.04

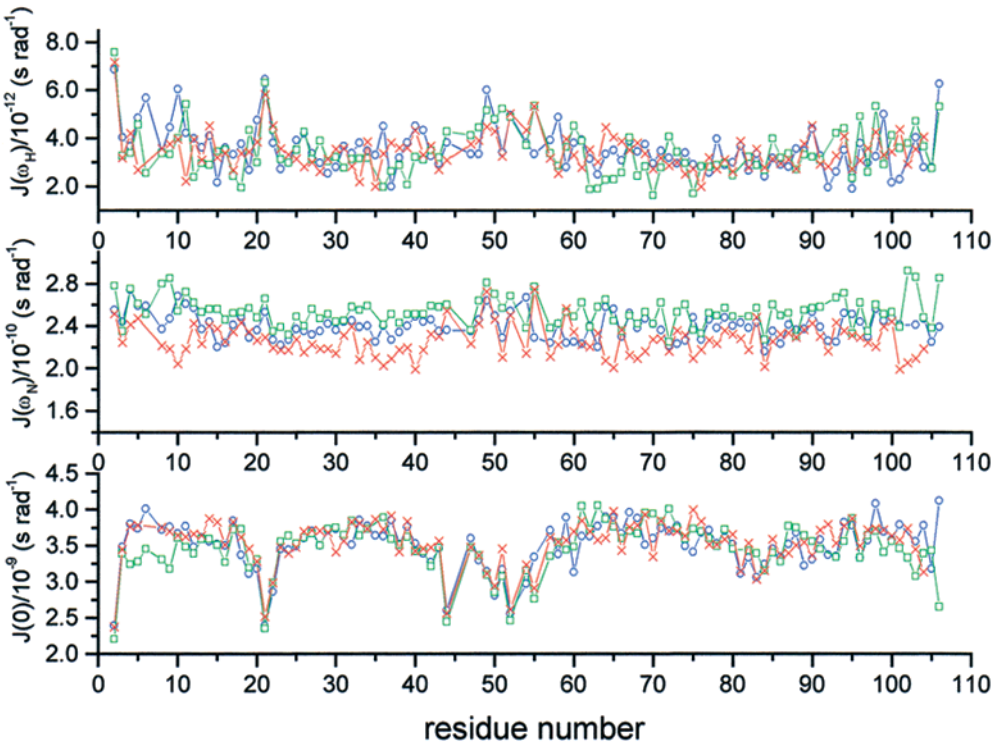

FIGURE 2: Spectral density function values for the $J(\omega_H)$, $J(\omega_N)$, and $J(0)$ terms at a 600 MHz proton Larmor frequency for oxidized (○), reduced (×), and oxidized R98C (□) cytochrome b_{562}.

The experimental data were then used to map the spectral density function values. This approach to the analysis of the ^{15}N relaxation data, originally proposed by Peng and Wagner (*29*), has the advantage over the ModelFree approach of not requiring any assumption about the tumbling motions of the molecule in solution. Since $\omega_H \approx 10\omega_N$, frequencies $\omega_H \pm \omega_N$ can be approximated to ω_H and the spectral density function values at the frequencies of interest can by approximated by the following expressions:

$$J_{eff}(0) = \frac{6R_2 - 3R_1 - \frac{18}{5}R_1(\mathrm{NOE} - 1)\frac{\gamma_N}{\gamma_H}}{(3d^2 + 4c^2)} \quad (9)$$

$$J(\omega_N) = \frac{4R_1}{3d^2 + 4c^2}\left[1 - \frac{7}{5}(\mathrm{NOE} - 1)\frac{\gamma_N}{\gamma_H}\right] \quad (10)$$

$$J(\omega_H) = 0.2R_1(\mathrm{NOE} - 1)\frac{4}{d^2}\frac{\gamma_N}{\gamma_H} \quad (11)$$

It should be noted that $J_{eff}(0)$ is used instead of $J(0)$ to denote that exchange contributions to R_2 have not been explicitly considered in the present analysis (*67*).

The values of the spectral density functions at $\omega = 0$, ω_N (60 MHz), and ω_H (600 MHz) are plotted in Figure 2 versus the residue number.

Rotational Diffusion Tensor and ModelFree Analysis. From the calculation of the inertia tensor, it is found that the molecule is asymmetric, as expected from its shape (the inertia tensor for oxidized cyt b_{562} has principal values in a 1.00:0.97:0.38 ratio). The diffusion tensor appears to be axial. If the rotational diffusion is anisotropic and not included in the analysis, erroneous conclusions about exchange rates would result. The introduced errors have been estimated by fitting simulated data, and it is observed that for a rigid nonspherical body, R_2 is underestimated by 20% for anisotropies $D_{||}/D_{\perp}$ equal to 2.0 (*44*). For moderate anisotropies (ca. 1.3), the order parameters remain insensitive to the choice of model (*68*), but the internal correlation time, τ_e, may be overestimated and the exchange contribution artificial. The asymmetry was verified further by determining the diffusion tensor from the R_2/R_1 ratio with the program *quadric_diffusion*. The calculation indicates a statistically better fit for the relaxation data by using the axially symmetric model over the isotropic model (F statistic > 3). No statistically significant improvement in the fully anisotropic model over axially symmetric diffusion was observed. We analyzed the relaxation data by using both the isotropic and axially symmetric models for the rotational diffusion tensor. In going from the isotropic to the axially symmetric case, we found no significant change in the results, but a better fit of the relaxation data was obtained with the axially symmetric model. We discuss below the results obtained for the axially symmetric case only. After optimization in the final stages of ModelFree calculations, $D_{||}/D_{\perp}$ ratios of 1.10 ± 0.05, 1.30 ± 0.06, and 1.19 ± 0.05 and τ_m values of 9.6 ± 0.6, 9.7 ± 0.4, and 9.2 ± 0.5 ns were found for oxidized cyt b_{562}, reduced cyt b_{562}, and R98C cyt b_{562}, respectively.

By analyzing the τ_m values of a group of proteins (*6*, *64*, *69*−*72*), determined experimentally by NMR, versus their molecular volumes (at normalized temperatures), we found that the present τ_m values are higher than expected. Since the protein tends to aggregate, care is taken to avoid this possibility. Literature data show that aggregation is prevented by a phosphate concentration of 500 mM and a protein concentration of <4 mM (*28*). ^{15}N R_1 and R_2 were measured at 500 MHz for oxidized cyt b_{562} in the protein concentration range of 0.5−1.8 mM, in 500 mM phosphate buffer at pH

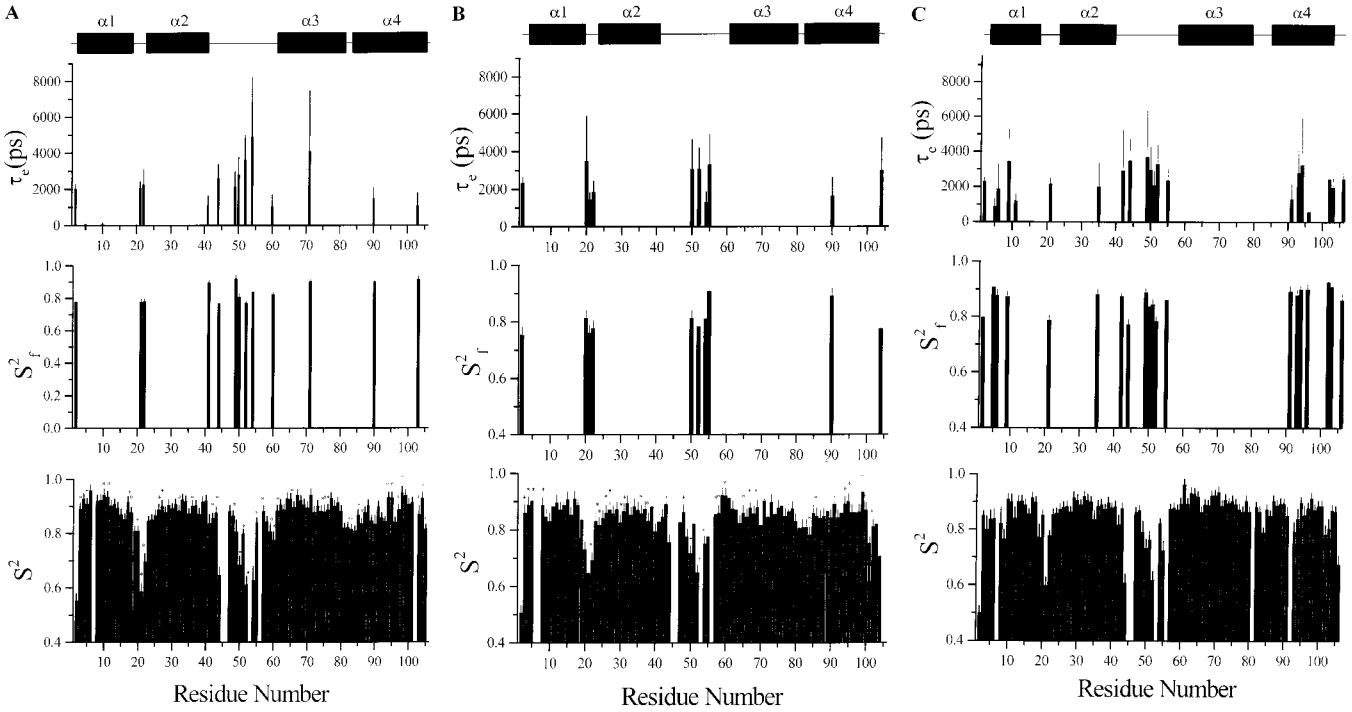

FIGURE 3: ModelFree parameters vs residue number for (A) oxidized, (B) reduced, and (C) oxidized R98C cytochrome b_{562}. The thinner lines indicate the error bar on the parameter values. The position of the helices with respect to the primary sequence is shown above the figure. Asterisks denote degenerate resonances for the two forms.

4.8. Within experimental error, the data are identical within this concentration range. Analysis of the relaxation data on the 0.5 mM protein sample provided a τ_m value of 9.1 ± 0.4 ns with an anisotropy $D_{||}/D_{\perp}$ of 1.21 ± 0.05. These values, if compared with the data at 1.8 mM protein, are consistent with a degree of association tending to zero. Moreover, no chemical shifts or line broadening of the cross-peaks in the $^{15}N-^{1}H$ HSQC spectra was monitored over the above range of protein concentrations for those residues that can be considered involved in the dimerization process, on the basis of the dimeric X-ray structure (*14*). Aggregation would determine changes in ^{15}N transverse relaxation rates and chemical shifts (*73*). The lack of any spectral change is again indicative of the absence of aggregation. Finally, when comparing the orientation of the principal axes of the diffusion tensor with the principal components of the inertia tensor calculated for the monomeric and dimeric forms of the molecule [the latter obtained from the crystal structure (*14*)], we found a very good agreement for the monomeric form (angle deviations of <15°), while a large discrepancy is calculated for the dimeric form. The same approach was previously used to provide evidence that cytochrome c' is monomeric in the solution state (*74*). Thus, it is concluded that the high value of τ_m is not due to aggregation, but arises from other effects such as the anisotropy of the molecular shape and the high concentration of the phosphate buffer. Indeed, from the structure of cyt b_{562}, it appears that most of the NH vectors are aligned along the main rotational diffusion axis. Since motions about the NH vectors do not contribute to relaxation, the data mostly describe motions around the transversal axis. The latter motions, judging from the shape of the molecule, are supposed to be much slower than those about the main diffusion axis. With respect to the overall tumbling motion, the latter situation can mimic a protein characterized by a slower isotropic motion. This interpretation is consistent with a large measured τ_m and a $D_{||}/D_{\perp}$ ratio of ∼1.

A further contribution to the above-mentioned deviation of the τ_m value derives from the high concentration of the phosphate buffer, which increases the viscosity of the solution. The effect of varying phosphate concentration on the τ_m value has been tested through NMRD measurements performed on bovine serum albumin, a protein which is known not to aggregate under the experimental conditions that were used (*59*). The τ_m value is found to increase by ∼70% when the phosphate concentration is increased from 0 to 500 mM. This figure can be considered a rough estimate of the effect of phosphate concentration on the τ_m of cyt b_{562} and accounts for most of the increase in the τ_m value. To our knowledge, no systematic studies on the effect of the buffer on protein tumbling are available in the literature.

The parameters characterizing the overall and internal mobility were obtained within the ModelFree approach (*43*) for 98 of 99 residues of oxidized cyt b_{562}; the signal of Arg 106 could not be fitted by any model. For reduced and R98C cyt b_{562}, 97 and 98 residues were fitted, respectively.

The average generalized order parameters S^2 values for all the characterized residues are 0.87 ± 0.08 for oxidized cyt b_{562}, 0.84 ± 0.07 for reduced cyt b_{562}, and 0.85 ± 0.07 for R98C cyt b_{562}. The S^2 for each residue, the internal correlation times τ_e, and the order parameter for the fast motions, S_f^2, are reported in Figure 3A (oxidized cyt b_{562}), Figure 3B (reduced cyt b_{562}), and Figure 3C (R98C cyt b_{562}). The pattern of S^2 values for the various residues in the three systems is similar. In all three cases, meaningful values (i.e., larger than their errors) for the correlation time for fast internal motions, τ_e, were found for residues belonging to loop 1 and loop 2 and for a few residues located in helices α1 and α4. Some of these residues also experience S_f^2 values of <1. Helices α1 and α4 of R98C cyt b_{562} present a larger

number of NH groups characterized by fast mobility with respect to the wild-type protein.

In oxidized cyt b_{562}, residue 59 exhibits an R_{ex} contribution to the transverse relaxation rate, arising from conformational exchange processes, of 2.55 ± 0.69 s^{-1}, while in the reduced protein, residue 101 exhibits an R_{ex} contribution to the transverse relaxation rate of 3.53 ± 0.60 s^{-1} and a τ_e value of 7.53 ± 2.52 s^{-1}. In R98C cyt b_{562}, no residues exhibit a detectable R_{ex} contribution through the measurements used for the ModelFree analysis.

CPMG R_2 Relaxation Data for Oxidized Proteins. Exchange processes in the millisecond to microsecond time scale can be observed as a contribution, R_{ex}, to the R_2 values measured in the T_2-CPMG experiments, increasing with τ_{CPMG} (see Materials and Methods) (*75*). The analysis was performed by measuring the transverse relaxation rates, R_2, of the backbone amide nitrogens as a function of τ_{CPMG} at different effective field strengths, ν_{eff}, according to eq 5. A dependence of R_2 with ν_{eff} indicates an exchange contribution to the transverse relaxation rate occurring with a rate on the same order as the ν_{eff}. To evaluate the exchange correlation time, τ_{ex}, the R_2 values have been fitted against ν_{eff} to eq 6. In both oxidized forms of cyt b_{562}, the transverse relaxation rates measured at the highest ν_{eff} possible are fairly homogeneous over the protein sequence with the exception of residues 21 and 22 in loop 1 and of some residues involved in loop 2 (see Figure 1). In oxidized cyt b_{562}, residues 54, 55, 57, 59, and 63, belonging to the final part of loop 2 and the beginning of helix α3, show a dependence of R_2 on ν_{eff}. Also, residues 9−11 and 17 (helix α1), 33, 35, and 40 (helix α2), and 87 and 106 display a dependence of R_2 on ν_{eff}. In oxidized R98C cyt b_{562}, residues showing R_2 rates higher than the average value are mainly present in helices α1 and α3. In these regions, residues 4−6, 9, 11, and 15−18 (helix α1) and 58, 66, 68, 69, and 71 (helix α3) also display a dependence of R_2 on ν_{eff}. In the other regions of the variant, residues showing a dependence of R_2 on ν_{eff} are 26, 30, and 33 (helix α2), 49 (loop 2), and 99 and 103 (helix α4). Residues exhibiting an exchange contribution in oxidized cyt b_{562} and R98C cyt b_{562} are listed in Table 2, together with the correlation time of the exchange process, τ_{ex}. The residues experiencing conformational exchange processes in both oxidized wild-type and variant forms of cyt b_{562} are schematically shown in panels A and B of Figure 4, respectively.

The CPMG experiments have also been carried out on the reduced protein. Reliable decay curves could not be measured in this case. The reason for this is the autoxidation of the sample, as documented elsewhere (*76*), during the longer time needed for this kind of measurement. Indeed, slight shift changes in the 2D spectra were observed between sets of experiments having different refocusing delays.

Table 2: Residues Exhibiting an Exchange Contribution to the ^{15}N Transverse Relaxation Rate in Oxidized Cyt b_{562} and R98C Cyt b_{562}[a]

	τ_{ex} (μs)			τ_{ex} (μs)	
residue	oxidized cyt b_{562}	oxidized R98C cyt b_{562}	residue	oxidized cyt b_{562}	oxidized R98C cyt b_{562}
4	*b*	174 ± 28	49	*b*	144 ± 28
5	*b*	175 ± 15	54	317 ± 110	*b*
6	*b*	178 ± 36	55	164 ± 98	*b*
9	382 ± 19	423 ± 38	57	159 ± 79	*b*
10	400 ± 94	*b*	58	*b*	366 ± 30
11	381 ± 56	415 ± 115	59	149 ± 70	*b*
15	*b*	177 ± 11	63	393 ± 60	*b*
16	*b*	139 ± 17	66	*b*	142 ± 30
17	178 ± 8	164 ± 17	68	*b*	378 ± 17
18	*b*	448 ± 85	69	*b*	361 ± 20
26	*b*	370 ± 18	71	*b*	144 ± 35
30	*b*	375 ± 44	87	125 ± 69	*b*
33	398 ± 120	143 ± 16	99	*b*	374 ± 17
35	418 ± 31	135 ± 69	103	*b*	176 ± 30
40	385 ± 11	*b*	106	245 ± 163	*b*

[a] The correlation time, τ_{ex}, in the exchange process, obtained through the fit to eq 5, is reported. [b] No exchange processes are observed in the 150−400 μs time range.

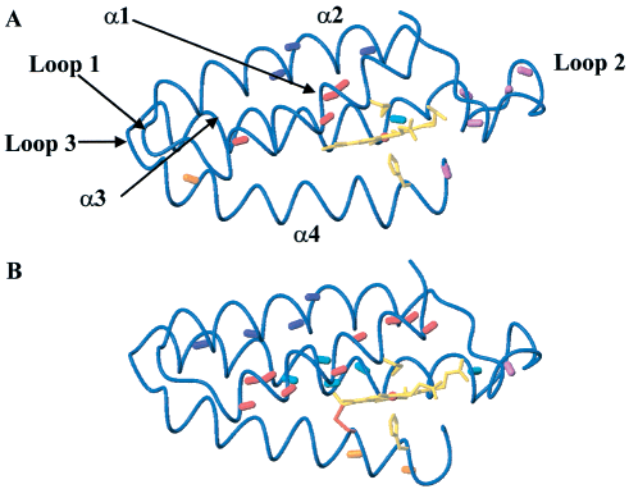

FIGURE 4: Mapping of ^{15}N mobility on the millisecond to microsecond time scale in the protein frame of the oxidized wild-type (A) and R98C (B) cytochrome b_{562} as it derives from T_2-CPMG experiments. The NH bonds experiencing exchange processes are depicted as lines colored by the following code based on the secondary structure: red, helix α1; violet, helix α2; pink, loop; cyan, helix α3; and orange, helix α4. The secondary structure elements are indicated.

DISCUSSION

E. coli cyt b_{562} consists of four long α-helices packed together in an antiparallel fashion corresponding to the well-known four-helix bundle topology. On the basis of relaxation data at two magnetic fields for 97−99 residues of 106, the analysis presented here finds that an axially symmetric diffusion tensor is appropriate for a description of the tumbling of the molecule in solution. It is interesting to observe that the relaxation data of cytochrome *c′*, displaying a fold very similar to that of cyt b_{562} but showing no significant sequence homology to cyt b_{562} (*77*), are reported to be better described by a fully anisotropic diffusion tensor (*74*).

The ModelFree analysis indicates that the three molecules investigated are particularly rigid on the picosecond to nanosecond time scale, as expected on the basis of their extensive helical structure. Average order parameter S^2 values of ∼0.90 are obtained for residues belonging to the helices. Larger mobility is observed for the terminal residues, as well as for residues belonging to loop 1 (residues 19−22), loop 2 (residues 41−45 and 49−57), and loop 3 (residues 81−83). Loops 1 and 2 are characterized by S^2 values as low as 0.59, and loop 3 is characterized by an average of ∼0.82

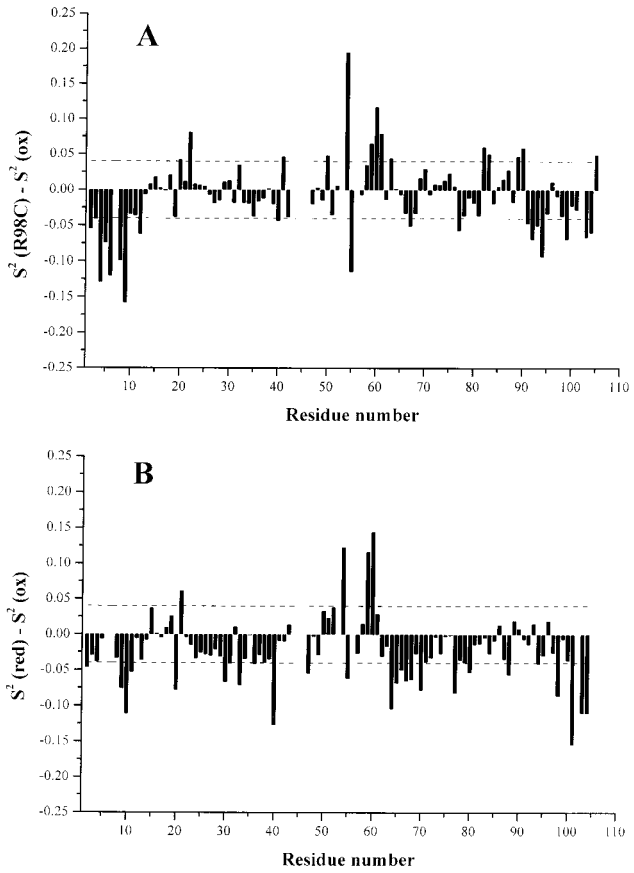

FIGURE 5: Differences in the order parameters (S^2) of the backbone nitrogens for (A) R98C minus wild-type cyt b_{562} and (B) reduced minus oxidized cytochrome b_{562} vs residue number. The dotted lines represent the sum of the average errors on the S^2 values of the two systems.

(Figure 3). Furthermore, these regions also display S_f^2 values different from 1, indicating the presence of very fast local motions characterized by correlation times of <20 ps (*78*). Mapping the values of the spectral density function at frequencies of 0, 60 ($=\omega_N$), and 600 MHz ($=\omega_H$) over the protein frame results in the loop regions being characterized by $J(0)$ values that are smaller than the average and by $J(\omega_H)$ values that are larger than the average (Figure 2). These two observations point again to larger backbone fluctuations on the picosecond to nanosecond time scale in these regions. No significant conformational exchange processes ($R_{ex} > 5$ s^{-1}) have been found by the ModelFree analysis, but motions on the millisecond to microsecond time scale have been detected for the oxidized proteins through CPMG experiments. These results are discussed in the following section.

Comparison between Oxidized Wild-Type and R98C Cytochrome b_{562}. The relaxation data (Figure 1) and S^2 values (Figure 5A) indicate that the mobilities of the oxidized wild-type and R98C cyt b_{562} are on average very similar on the picosecond to nanosecond time scale. However, a detailed analysis over the whole amino acid sequence reveals some significant local differences. It appears that the variant has more higher-mobility residues than the wild-type protein.

Residues 4−12 (belonging to helix α1) and 91−103 (helix α4) contain the axial ligands to the iron and are significantly more mobile in R98C cyt b_{562} than in the wild-type protein. The latter exhibits average S^2 values of 0.93 and 0.90 and the former values of 0.84 and 0.85 (Figure 3). These observations are supported by S_f^2 values different from 1 in R98C cyt b_{562}, indicating the presence of relatively fast local motions which contribute significantly to relaxation. Moreover, it has been shown previously (*15*, *16*) that the HN protons of residues 2−7 in R98C cyt b_{562} are more exchangeable with bulk solvent than those in the wild-type protein. Apparently, the introduction of a covalent bond between the heme and helix α4 causes an increase in mobility on the sub-nanosecond time scale in the latter helix. Such mobility is extended to helix α1 through the coordination bond between the iron and Met 7. The effect can be ascribed reasonably to strain introduced by the thioether bond.

Residues 58−61 also show a slight difference in mobility. The local S^2 values of wild-type and R98C cyt b_{562} are 0.83 and 0.90 on average, respectively. This difference is related to the secondary structure, as these residues belong to helix α3 in R98C cyt b_{562} but not in the wild-type protein (*15*, *16*).

Another approach to evaluating differences in mobility between two related species is that of calculating the difference in entropy ΔS from S^2 values, according to eq 4. The change in entropy is related to the ratio of the square root of the order parameter S, evaluated for each NH group and summed for all the NHs detected in the two forms. While the average S^2 values are close for the two states, meaningful differences can be detected, as shown in Figure 5A. There are 96 residues having S^2 values of <0.95, and the entropy change was estimated to be 74 ± 25 J mol^{-1} K^{-1}. This value indicates a globally higher disorder in R98C cyt b_{562}.

In comparison to the wild-type protein, R98C cytochrome is more stable toward thermal and chemical denaturation ($\Delta\Delta G_{D-N}^{H_2O} = 5.6$ kJ/mol) (*22*). This feature is not reflected in an increased rigidity. While the thioether bond increases resistance to thermal and chemical unfolding, it also introduces structural strains that amplify backbone atom motions on the sub-nanosecond time scale for the region close to the heme axial ligands. Interestingly, this effect is most noticeable on helix 1, trans to the new covalent bond. This region, which evolved to bind the heme 2-vinyl group, now has to accommodate the 2-methyl group of the heme.

Residues experiencing conformational exchange on the millisecond to microsecond time scale were identified through analysis of the dependence of transverse relaxation rates on the delay of the spin-echo pulse train. The total number of backbone nitrogens participating in such exchange processes is larger in R98C cyt b_{562} than in the wild-type protein (see Table 2 and Figure 4). In particular, most residues belonging to helix α1 of R98C cyt b_{562} display a dependence of R_2 values on τ_{CPMG}. Only four do in the case of the wild-type protein. Another difference is observed in loop 2 where wild-type cyt b_{562} exhibits a higher mobility on this time scale (*15*). Finally, in the R98C protein, residues 99 and 103 belonging to helix α4 experience exchange processes which vary from those of the wild-type protein. In general, the behavior in the millisecond to microsecond time scale is similar to that observed on the sub-nanosecond time scale.

Comparison between Oxidized and Reduced Wild-Type Cytochrome b_{562}. Analysis of the relaxation data for the two redox forms of cyt b_{562} shows that the reduced form has

generally lower S^2 values for essentially all the residues. Exceptions occur in loop 2 (Figures 1 and 5B).

If eq 4 is used to estimate the NH fluctuation contribution to $\Delta S°$, a value of 168 ± 22 J mol^{-1} K^{-1} is obtained from 96 NH pairs with S^2 values of <0.95. The positive value indicates that the entropic contribution from backbone mobility favors the reduced state. This behavior is the opposite of that observed for mitochondrial cytochrome *c* (*70*) and cytochrome b_5 (*65*), but is the same as that for the low-potential cytochrome c_{553} from *D. vulgaris* (*79*). Thus, the entropic contribution calculated from the S^2 data is found to be variable among these proteins. It also shows similarity in the magnitude of the overall thermodynamic values of homologous systems, but it is clear that this is only one of the contributions to $\Delta S°$. Indeed, it has been proposed that the global entropy change is mainly determined by solvation effects (*80*, *81*).

Reduction of cyt b_{562} increases its stability toward unfolding, the reduced protein being ~25 kJ/mol more stable than the oxidized protein (*26*). Our results show that the reduced form is slightly more mobile than the oxidized protein. Unfortunately, the present system is not suited for a comparison of the backbone dynamics on the microsecond to millisecond time scale, which has been correlated with the protein local stability (*82*).

CONCLUSIONS

In this work, the backbone dynamics of the oxidized and reduced cyt b_{562}, as well as of the oxidized R98C variant, have been analyzed and compared to evaluate the effects of redox or chemical modification on protein mobility. The three proteins display very similar global dynamic behavior on the picosecond to nanosecond time scale. However, some local differences are observed. The regions of residues 4−12 and 91−104 belonging to helices α1 and α4, respectively, result in a more mobile oxidized R98C variant with respect to the oxidized wild-type protein. In addition, a higher degree of conformational exchange has been observed in the same regions for the R98C variant. Thus, the new covalent link forces the protein into a state characterized by higher mobility. This may be a consequence of strain produced by an artificial covalent bond between the heme and the protein matrix. Similarly, the reduction process does not determine large changes in mobility on the picosecond to nanosecond time scale, although slightly lower S^2 values are observed for the reduced protein. The latter observation cannot be generalized as the difference in backbone mobility between the oxidized and reduced cytochromes has been found to be either positive or negative. Finally, entropy estimates obtained from order parameters indicate that picosecond to nanosecond time scale motions contribute to the stabilization of the variant and the reduced forms of cyt b_{562}.

ACKNOWLEDGMENT

We thank M. Bruschi of the CNRS (Marseille, France) for providing the *D. vulgaris* iron hydrogenase and Dr. Isabella C. Felli for help during the acquisition of the NMR spectra.

SUPPORTING INFORMATION AVAILABLE

Tables and plots containing experimental ^{15}N relaxation data for the resolved ^{15}N−^{1}H peaks in the HSQC spectra of oxidized, reduced, and R98C variant cyt b_{562}. This material is available free of charge via the Internet at http://pubs.acs.org.

REFERENCES

1. Gerstein, M., Lesk, A. M., and Clothia, C. (1994) *Biochemistry 33*, 6739−6749.
2. Dobson, C. M. (1993) *Curr. Biol. 3*, 530−532.
3. London, R. E. (1989) *Methods Enzymol. 176*, 358−375.
4. Pedersen, T. G., Sigurskjold, B. W., Andersen, K. V., Kjaer, M., Poulsen, F. M., Dobson, C. M., and Redfield, C. (1991) *J. Mol. Biol. 218*, 413−426.
5. Kay, L. E., Torchia, D. A., and Bax, A. (1989) *Biochemistry 28*, 8972−8979.
6. Bertini, I., Luchinat, C., Niikura, Y., and Presenti, C. (2000) *Proteins: Struct., Funct., Genet. 41*, 75−85.
7. Arnesano, F., Banci, L., Bertini, I., Koulougliotis, D., and Monti, A. (2000) *Biochemistry 39*, 7117−7130.
8. Lipari, G., and Szabo, A. (1982) *J. Am. Chem. Soc. 104*, 4559−4570.
9. Lipari, G., and Szabo, A. (1982) *J. Am. Chem. Soc. 104*, 4546−4559.
10. Wagner, G., Hyberts, S., and Peng, J. W. (1993) in *NMR of Proteins*, pp 220−257, Macmillan Press, New York.
11. Akke, M., and Palmer, A. G., III (1996) *J. Am. Chem. Soc. 118*, 911−912.
12. Szyperski, T., Luginbuhl, P., Otting, G., Güntert, P., and Wüthrich, K. (1993) *J. Biomol. NMR 3*, 151−164.
13. Ishima, R., and Nagayama, K. (1995) *Biochemistry 34*, 3162−3171.
14. Hamada, K., Bethge, P. H., and Mathews, F. S. (1995) *J. Mol. Biol. 247*, 947−962.
15. Arnesano, F., Banci, L., Bertini, I., Faraone-Mennella, J., Rosato, A., Barker, P. D., and Fersht, A. R. (1999) *Biochemistry 38*, 8657−8670.
16. Arnesano, F., Banci, L., Bertini, I., Ciofi-Baffoni, S., de Lumley Woodyear, T., Johnson, C. M., and Barker, P. D. (2000) *Biochemistry 39*, 1499−1514.
17. Moore, G. R., and Pettigrew, G. W. (1990) *Cytochromes c; Evolutionary, Structural and Physicochemical Aspects*, Springer-Verlag, Berlin.
18. Canters, G. W., and Van de Kamp, M. (1992) *Curr. Biol. 2*, 859−869.
19. Zhou, J. S., and Kostic, N. M. (1992) *J. Am. Chem. Soc. 114*, 3562−3563.
20. Hake, R., McLendon, G., Corin, A., and Holzschu, D. (1992) *J. Am. Chem. Soc. 114*, 5442−5443.
21. Peerey, L. M., Brothers, H. M. I., Hazzard, J. T., Tollin, G., and Kostic, N. M. (1991) *Biochemistry 30*, 9297−9304.
22. Corin, A., McLendon, G., Zhang, Q., Hake, R., Falvo, J., Lu, K. S., Ciccarelli, R. B., and Holzschu, D. (1991) *Biochemistry 30*, 11585−11595.
23. Walker, M. C., and Tollin, G. (1991) *Biochemistry 30*, 5546−5555.
24. Akke, M., Brüschweiler, R., and Palmer, A. G., III (1993) *J. Am. Chem. Soc. 115*, 9832−9833.
25. Stone, M. J. (2001) *Acc. Chem. Res. 34*, 379−388.
26. Wittung-Stafshede, P., Gray, H. B., and Winkler, J. R. (1997) *J. Am. Chem. Soc. 119*, 9562−9563.
27. Barker, P. D., Nerou, E. P., Freund, S. M. V., and Fearnley, I. M. (1995) *Biochemistry 34*, 15191−15203.
28. Wu, J. Z., La Mar, G. N., Yu, L. P., Lee, K. B., Walker, F. A., Chiu, M. L., and Sligar, S. G. (1991) *Biochemistry 30*, 2156−2165.
29. Peng, J. W., and Wagner, G. (1992) *J. Magn. Reson. 98*, 308−332.
30. Palmer, A. G., III, Skelton, N. J., Chazin, W. J., Wright, P. E., and Rance, M. (1992) *Mol. Phys. 75*, 699−711.
31. Kay, L. E., Nicholson, L. K., Delaglio, F., Bax, A., and Torchia, D. A. (1992) *J. Magn. Reson. 97*, 359−375.
32. Barbato, G., Ikura, M., Kay, L. E., Pastor, R. W., and Bax, A. (1992) *Biochemistry 31*, 5269−5278.

33. Grzesiek, S., and Bax, A. (1993) *J. Am. Chem. Soc. 115*, 12593−12594.
34. Peng, J. W., and Wagner, G. (1994) *Methods Enzymol. 239*, 563−596.
35. Piotto, M., Saudek, V., and Sklenar, V. (1992) *J. Biomol. NMR 2*, 661−666.
36. Marion, D., and Wüthrich, K. (1983) *Biochem. Biophys. Res. Commun. 113*, 967−974.
37. Marquardt, D. W. (1963) *J. Soc. Ind. Appl. Math. 11*, 431−441.
38. Press, W. H., Flannery, B. P., Teukolsky, S. A., and Vetterling, W. T. (1988) *Numerical Recipes in C: The Art of Scientific Computing*, Cambridge University Press, New York.
39. Palmer, A. G., III, Rance, M., and Wright, P. E. (1991) *J. Am. Chem. Soc. 113*, 4371−4380.
40. Peng, J. W., and Wagner, G. (1992) *Biochemistry 31*, 8571−8586.
41. Zinn-Justin, S., Berthault, P., Guenneugues, M., and Desvaux, H. (1997) *J. Biomol. NMR 10*, 363−372.
42. Abragam, A. (1961) *The Principles of Nuclear Magnetism*, Oxford University Press, Oxford, U.K.
43. Mandel, M. A., Åkke, M., and Palmer, A. G., III (1995) *J. Mol. Biol. 246*, 144−163.
44. Schurr, J. M., Babcock, H. P., and Fujimoto, B. S. (1994) *J. Magn. Reson., Ser. B 105*, 211−224.
45. Tjandra, N., Wingfield, P., Stahl, S., and Bax, A. (1996) *J. Biomol. NMR 8*, 273−284.
46. Luginbuhl, P., Pervushin, K. V., Iwai, H., and Wüthrich, K. (1997) *Biochemistry 36*, 7305−7312.
47. Tjandra, N., Feller, S. E., Pastor, R. W., and Bax, A. (1995) *J. Am. Chem. Soc. 117*, 12562−12566.
48. Tjandra, N., Grzesiek, S., and Bax, A. (1996) *J. Am. Chem. Soc. 118*, 6264−6272.
49. Hiyama, Y., Niu, C. H., Silverston, J. V., Bavoso, A., and Torchia, D. A. (1988) *J. Am. Chem. Soc. 110*, 2378−2383.
50. Roberts, J. E., Harbison, G. S., Munowitz, M. G., Herzfeld, J., and Griffin, R. G. (1987) *J. Am. Chem. Soc. 109*, 4163−4169.
51. Case, D. A. (1999) *J. Biomol. NMR 15*, 95−102.
52. Kroenke, C. D., Rance, M., and Palmer, A. G., III (1999) *J. Am. Chem. Soc. 121*, 10119−10125.
53. Cornilescu, G., and Bax, A. (2000) *J. Am. Chem. Soc. 122*, 10143−10154.
54. Woessner, D. E. (1962) *J. Chem. Phys. 3*, 647−652.
55. Halle, B., and Wennerström, H. (1981) *J. Chem. Phys. 75*, 1928−1943.
56. Yang, D., and Kay, L. E. (1996) *J. Mol. Biol. 263*, 369−382.
57. Palmer, A. G., III, Williams, J., and McDermott, A. (1996) *J. Phys. Chem. 100*, 13293−13310.
58. Luz, Z., and Meiboom, S. (1963) *J. Chem. Phys. 39*, 370.
59. Bertini, I., Fragai, M., Luchinat, C., and Parigi, G. (2000) *Magn. Reson. Chem. 38*, 543−550.
60. Bertini, I., and Luchinat, C. (1996) *NMR of paramagnetic substances*, Coordination Chemistry Review 150, Elsevier, Amsterdam.
61. Banci, L., Bertini, I., and Luchinat, C. (1991) *Nuclear and electron relaxation. The magnetic nucleus-unpaired electron coupling in solution*, VCH, Weinheim, Germany.
62. Banci, L. (1993) in *Biological Magnetic Resonance* (Berliner, L. J., and Reuben, J., Eds.) pp 79−111, Plenum, New York.
63. Banci, L., Felli, I. C., and Koulougliotis, D. (1998) *J. Biomol. NMR 12*, 307−318.
64. Banci, L., Bertini, I., Cavazza, C., Felli, I. C., and Koulougliotis, D. (1998) *Biochemistry 37*, 12320−12330.
65. Dangi, B., Blankman, J., Miller, C. J., Volkman, B. F., and Guiles, R. D. (1998) *J. Phys. Chem. B 102*, 8201−8208.
66. Solomon, I. (1955) *Phys. Rev. 99*, 559−565.
67. Peng, J. W., and Wagner, G. (1995) *Biochemistry 34*, 16733−16752.
68. Dangi, B., Sarma, S., Yan, C., Banville, D. L., and Guiles, R. D. (1998) *Biochemistry 37*, 8289−8302.
69. Banci, L., Bertini, I., Cramaro, F., Del Conte, R., Rosato, A., and Viezzoli, M. S. (2000) *Biochemistry 39*, 9108−9118.
70. Fetrow, J. S., and Baxter, S. M. (1999) *Biochemistry 38*, 4480−4492.
71. Sahu, S. C., Bhuyan, A. K., Majumdar, A., and Ugdaonkar, J. B. (2000) *Proteins: Struct., Funct., Genet. 41*, 460−474.
72. Clore, G. M., Driscoll, P. C., Wingfield, P. T., and Gronenborn, A. M. (1990) *Biochemistry 29*, 7387−7401.
73. Pfuhl, M., Chen, H. A., Kristensen, S. M., and Driscoll, P. C. (1999) *J. Biomol. NMR 14*, 307−320.
74. Tsan, P., Hus, J. C., Caffrey, M., Marion, D., and Blackledge, M. (2000) *J. Am. Chem. Soc. 122*, 5603−5612.
75. Orekhov, V. Y., Pervushin, K. V., and Arseniev, A. S. (1994) *Eur. J. Biochem. 219*, 887−896.
76. Moore, G. R., Williams, R. J., Peterson, J., Thomson, A. J., and Mathews, A. J. (1985) *Biochim. Biophys. Acta 829*, 83−96.
77. Mathews, F. S. (1985) *Prog. Biophys. Mol. Biol. 45*, 1−56.
78. Clore, G. M., Szabo, A., Bax, A., Kay, L. E., Driscoll, P. C., and Gronenborn, A. M. (1990) *J. Am. Chem. Soc. 112*, 4989−4991.
79. Blanchard, L., Blackledge, M. J., Marion, D., and Guerlesquin, F. (1996) *FEBS Lett. 389*, 203−209.
80. Bertrand, P., Mbarki, O., Asso, M., Blanchard, L., Guerlesquin, F., and Tegoni, M. (1995) *Biochemistry 34*, 11071−11079.
81. Battistuzzi, G., Borsari, M., Loschi, L., Righi, F., and Sola, M. (1999) *J. Am. Chem. Soc. 121*, 501−506.
82. Ishima, R., and Torchia, D. A. (2000) *Nat. Struct. Biol. 7*, 740−743.

BI0101300